The Astrophysical Journal, 906:24 (13pp), 2021 January 1 https://doi.org/10.3847/1538-4357/abc68f

A VLBA Survey of Radio Stars in the Orion Nebula Cluster. II. Astrometry

Sergio A. Dzib[1], Jan Forbrich[2,3], Mark J. Reid[3], and Karl M. Menten[1]
[1] Max-Planck-Institut für Radioastronomie, Auf dem Hügel 69, D-53121 Bonn, Germany; sdzib@mpifr-bonn.mpg.de
[2] Centre for Astrophysics Research, University of Hertfordshire, College Lane, Hatfield AL10 9AB, UK
[3] Center for Astrophysics | Harvard & Smithsonian, 60 Garden Street, MS 72, Cambridge, MA 02138, USA
Received 2020 May 22; revised 2020 October 28; accepted 2020 October 29; published 2021 January 4

Abstract

From Very Long Baseline Array (VLBA) observations we previously identified a population of 123 young stellar systems with nonthermal radio emission toward the core of the Orion Nebula Cluster (ONC). We find optical sources in the Gaia DR2 catalog for 34 of them within 0.″2 of the radio positions. Most of the radio sources are likely companions of Gaia detections. However, there are 11 stars whose VLBA positions differ from Gaia by <1.6 mas, and some of these radio sources probably are the direct counterparts of the optical stars. We are able to obtain radio proper motions for 23 stars. Combining the stellar proper motions derived from the VLBA and Gaia DR2 data we find the global motion and velocity dispersion of the ONC to be $(\mu_{\alpha}*, \mu_{\delta}) = (1.20 \pm 0.09, 0.18 \pm 0.09)$ mas yr^{-1} and $(\sigma_{\mu_{\alpha}} *, \sigma_{\mu_{\delta}}) = (0.84 \pm 0.09, 1.30 \pm 0.09)$ mas yr^{-1}. Finally, we looked for ordered motions by estimating the means of scalar and vectorial products, which results in $\overline{\boldsymbol{v} \cdot \hat{\boldsymbol{r}}} = -0.61 \pm 1.00$ km s^{-1} and $\overline{\boldsymbol{v} \times \hat{\boldsymbol{r}}} = 0.57 \pm 0.95$ km s^{-1}. These do not show indications that the young stellar cluster is in expansion, contraction, or rotation.

Unified Astronomy Thesaurus concepts: Star formation (1569); Radio astrometry (1337); Non-thermal radiation sources (1119)

1. Introduction

The Orion Nebula Cluster (ONC), at a distance of about 400 pc (Menten et al. 2007; Kim et al. 2008; Kounkel et al. 2017), is the nearest region in which massive stars have formed <2 million years ago (Muench et al. 2008). It contains a rich stellar population composed of a few high-mass stars, which already are on the main sequence, and many low-mass pre-main-sequence young stellar objects (YSOs). With its ∼3500 members, the ONC is the most extensively studied young, partially embedded, star cluster (e.g., Hillenbrand 1997; Getman et al. 2005; Da Rio et al. 2012).

The Kleinmann–Low (KL) Nebula is located a fraction of a parsec behind the ONC (Zuckerman 1973; Genzel & Stutzki 1989). Within it, the deeply embedded Becklin–Neugebauer object (BN) and a number of other embedded near-infrared (NIR) sources are evidence for more recent star formation.

At radio wavelengths, a rich population of compact sources has been found, many of which represent young stars in the ONC that are visible at NIR and optical wavelengths whereas others are associated with optically invisible NIR sources in the KL region. In the radio and the NIR range, the most prominent radio source in this region is BN (Churchwell et al. 1987; Garay et al. 1987; Zapata et al. 2004; Kounkel et al. 2014; Forbrich et al. 2016). Some very deeply embedded sources show no optical or even infrared counterparts at all, but are still detected at X-ray and/or radio wavelengths (see, e.g., Menten & Reid 1995; Forbrich et al. 2008). Multiepoch high-resolution interferometric studies of these YSOs at radio wavelengths have helped to constrain the ONC distance (Hirota et al. 2007; Menten et al. 2007; Sandstrom et al. 2007; Kounkel et al. 2017), study their kinematics (e.g., Dzib et al. 2017), and uncover sources related to the dynamical decay, some 500 yr ago, of a multiple stellar system within the KL Nebula (e.g., Gómez et al. 2008; Rodríguez et al. 2017, 2020, and references therein).

Magnetically active young low-mass stars produce non-thermal radio emission from their coronae (Feigelson & Montmerle 1999). The coronae have sizes of at most a few stellar radii (Güdel 2002), and have high brightness temperatures (>10^6 K). Thus, they provide excellent targets for observations with the Very Long Baseline Interferometry technique (VLBI), which provides astrometric precision of the order of tens of microarcseconds (Reid & Honma 2014).

In order to characterize the nonthermal population of the ONC and study its kinematics, we initiated a campaign of high angular resolution observations with the Very Long Baseline Array (VLBA) targeting all 557 compact radio sources[4] known to exist in the region (e.g., Forbrich et al. 2016; Dzib et al. 2017). In a companion paper we focused on the detection criteria and sample definition (Paper I, Forbrich et al. 2021), and in future articles we shall discuss in detail the properties of the whole sample. In this paper we report the measured positions and proper motions for sources detected in two or more epochs.

2. Observations

A full description of the observations is given in Paper I, and only a brief summary follows. Four C-band observations, centered at 7.196 GHz, were carried out with the VLBA in three different years (Table 1). Three of these observations were arranged to be made at the same day of the year, October 26, in 2015, 2017, and 2018. The observations in 2015 and 2017 resulted in larger synthesized beam sizes because the array's most outlying antennas (Maunakea or St. Croix), which provide the longest baselines, were not operational (see Paper I for full details). An additional epoch was obtained on 2017 October 27. Given the low decl. of the ONC, the synthesized

[4] We use the nomenclature [FRM2016] followed by the catalog number in Forbrich et al. (2016) to name these sources.

Table 1
Observed Epochs

Epoch	Date yyyy/mm/dd	Synthesized Beam ($\theta_{maj} \times \theta_{min}$; P.A.)	$\#_{Ant.}$
1	2015/10/26	$0\farcs00471 \times 0\farcs00165$; $+22\fdg1$	8
2	2017/10/26	$0\farcs00435 \times 0\farcs00135$; $-17\fdg3$	7
3	2017/10/27	$0\farcs00407 \times 0\farcs00139$; $-17\fdg8$	7
4	2018/10/26	$0\farcs00283 \times 0\farcs00116$; $-02\fdg1$	10

Note. Columns are (left to right) epoch of the observation, civil date, FWHM major and minor axes and position angle (E of N) of the synthesized beam, and the number of antennas used.

beam is elongated in the north–south direction, resulting in a better astrometric precision in R.A. than in the decl. direction.

The 557 known sources within the primary beam were correlated using the DiFX software correlator (Deller et al. 2011), which generates separate visibility data sets for each source position. The phase calibrator was the quasar J0541 −0541 correlated at the position R.A. = $05^h41^m38\fs083384$; decl. = $-05°41'49\farcs42839$ i.e., with angular separations from the ONC of $1\fdg6$ in R.A. and $0\fdg3$ in decl. The correlated position was 0.24 mas off in R.A. and 0.07 mas off in decl. from the most recent determined position of this quasar provided by the AstroGeo website,[5] and source positions in this paper have been corrected to reflect the new calibrator position.

Data calibration was performed using the Astronomical Image Processing System software (Greisen 2003). The calibration was done following standard procedures and images of detected sources were produced with pixel sizes of 50 μas. See Paper I for further information on the image processing and a detailed description on detection criteria. Images are exported in FITS format and read into the CASA software. General properties of the images are listed in Table 1. Source positions are measured with the CASA task *imfit*. The formal position errors derived from *imfit* range from 0.02 to 0.60 mas. However, we note that at this frequency, systematic residual position errors are expected to be ≈0.1 mas per degree-of-separation between the phase calibrator and the target (Reid et al. 2017); however, it is not clear if this systematic residual is direction dependent. In our case, we have to consider a total systematic error of 0.16 mas appropriate for the $1\fdg6$ separation between the phase calibrator and the ONC. The 0.16 mas error affects both coordinates, and for each coordinate we consider $0.16\ \mathrm{mas}/\sqrt{2} \simeq 0.11$ mas. This value was added in quadrature to the formal position errors derived from *imfit*.

3. Results

In Paper I, we described the criteria used for source detection. A total of 123 stellar systems were detected with brightness levels >6.5 times the noise. Most of the VLBA detections match this criterion in only one epoch. However, once the source has been clearly detected in at least two epochs, we have lowered the detection criterion to be >6 times the noise for the remaining epochs if the position is in line with the clear detections. In one case, [FRM2016] 382, with just a single VLBA detection at >6.5 times the noise level, we also used a threshold of 6.0 times the noise since its position is consistent with the position of a star in the Gaia DR2 catalog.

The measured source positions are listed in Table 2. In a small number of cases we detected multiple sources related to a single source found in the lower resolution VLA observations.

3.1. Detection of Multiple Sources

In the images of [FRM2016] 414 only one source is detected in epochs 1, 2, and 3. However, at epoch 4, two compact radio sources with a separation, $\Delta\theta$, of $0\farcs22$ are clearly detected. Given this large separation, compared with the angular resolution, we confirm that the radio sources detected at epochs 1 and 2 are associated with the eastern source in epoch 4, while the source at epoch 3 is associated with the western source in epoch 4. We refer to the source detected in three epochs as [FRM2016] 414-1 and the source detected in two epochs as [FRM2016] 414-2.

Similarly, source [FRM2016] 177 appears as a single source in epoch 1, while in epoch 4 two sources are clearly detected with a separation of 23.2 mas. A visual inspection of the images allows us to associate the southern source at epoch 4 with the source detected at epoch 1. We refer to southern and northern sources in epoch 4 as [FRM2016] 177-1 and [FRM2016] 177-2, respectively.

Two VLBA detections are related to the VLA source [FRM2016] 2; both were single detections in epochs 3 and 4. The source detected in epoch 4 is separated from the source in epoch 3 by 20.6 mas. As we will discuss later we discard the possibility of a fast moving source since the last detection in epoch 4 is only 1.6 mas from a source in the Gaia DR2 catalog, which has a small proper motion of 1.64 ± 0.10 mas yr^{-1}, indicating that the radio detections are from two different sources. As in the previous cases, we named these sources [FRM2016] 2-1 and [FRM2016] 2-2.

3.2. Proper Motions

The observations were scheduled on nearly the same day of the year in order to remove the effects of parallax from estimates of proper motion. This allowed us to estimate motions with a minimum of two epochs separated by at least 1 yr. For those sources detected in three or four epochs, the motion fits produced a reduced χ^2 near unity, indicating that our error estimates are realistic. Three exceptions, [FRM2016] 184, and 211, are discussed in Section 4.5, where we also discuss the three sources with proper motions >10 mas yr^{-1} ([FRM2016] 18, 137, and 198). The fitted proper motions for 23 sources are listed in Table 3 and plotted in Figure 1.

4. Discussion

In this section, we compare our results with previous VLBA observations and to Gaia DR2 astrometry. The astrometric precision from our observations is similar to those achieved by Gaia. A comparison of positions and proper motion measurements from both telescopes can give us clues as to the nature of the detected sources, may show systematic differences between the results from different telescopes, and allow us to study the kinematics of the ONC.

[5] This website (http://astrogeo.org/) provides a catalog of accurate positions for ∼17,000 extragalactic sources with compact radio emission. The positions are updated four times per year. We have consulted the current catalog *rfc_2020c* released in 2020 September 23. The position of J0541−0541 is listed as R.A. = $05^h41^m38\fs083368 \pm 0\fs000007$; decl. = $-05°41'49\farcs42846 \pm 0\farcs00011$.

Table 2
Positions of Detected Sources in the VLBA Images and their Formal Errors as Derived from *Imfit*

[FRM2016]	Epoch	α_{J2000} 5^h	σ_α μs	δ_{J2000} -5°	σ_δ μas	*Gaia* ID	$\Delta\theta$ (mas)	$\Delta\alpha$ (mas)	$\Delta\delta$ (mas)
2-1	3	$34^m55^s.975458$	10	$23'13''.02414$	330	3017364613086735360	22.4 ± 0.3	16.1 ± 0.3	15.6 ± 0.3
2-2	4	$34^m55^s.974448$	1	$23'13''.03823$	44	3017364613086735360	1.5 ± 0.3	-0.6 ± 0.3	1.3 ± 0.3
10	4	$35^m06^s.283539$	1	$22'02''.66564$	114	3017364303848915072	6.6 ± 1.0	2.3 ± 1.2	6.1 ± 1.0
11	3	$35^m06^s.416885$	5	$24'21''.34747$	200	⋯	⋯	⋯	⋯
14	2	$35^m07^s.243891$	7	$22'26''.30111$	324	⋯	⋯	⋯	⋯
18	1	$35^m09^s.675491$	5	$23'55''.91216$	203	⋯	⋯	⋯	⋯
	2	$35^m09^s.676642$	10	$23'55''.93895$	480	⋯	⋯	⋯	⋯
21	$2+3$	$35^m09^s.769705$	5	$23'26''.88897$	341	3017363994611276032	1.0 ± 0.4	0.1 ± 0.3	0.9 ± 0.4
22	3	$35^m09^s.769946$	3	$21'28''.34796$	168	3017364406917802752	5.7 ± 1.6	-0.6 ± 1.7	5.4 ± 1.6
24	1	$35^m09^s.882645$	10	$23'38''.33131$	468	⋯	⋯	⋯	⋯
25	$2+3$	$35^m10^s.043939$	7	$21'21''.93669$	414	⋯	⋯	⋯	⋯
30	2	$35^m10^s.252267$	10	$21'57''.11309$	301	3017364406926998784[a]	148.8 ± 0.8	-148.6 ± 0.8	7.0 ± 1.1
32	$2+3$	$35^m10^s.494684$	10	$22'45''.75147$	361	3017364235129434624	26.7 ± 0.6	1.1 ± 0.6	-26.7 ± 0.6
35	$2+3$	$35^m10^s.597692$	7	$22'55''.66427$	294	⋯	⋯	⋯	⋯
37	3	$35^m10^s.736683$	6	$23'44''.72569$	278	3017363994611283840	56.8 ± 0.4	36.8 ± 0.3	-43.3 ± 0.4
42	4	$35^m10^s.940386$	2	$23'26''.41294$	168	⋯	⋯	⋯	⋯
47	$2+3$	$35^m11^s.255552$	12	$22'16''.80621$	543	⋯	⋯	⋯	⋯
53	4	$35^m11^s.562674$	2	$24'48''.09454$	138	⋯	⋯	⋯	⋯
55	3	$35^m11^s.615114$	5	$20'22''.21699$	225	⋯	⋯	⋯	⋯
64	3	$35^m11^s.725033$	7	$25'12''.78408$	385	⋯	⋯	⋯	⋯
66	1	$35^m11^s.804276$	3	$21'49''.26414$	129	⋯	⋯	⋯	⋯
	2	$35^m11^s.804447$	1	$21'49''.26663$	74	⋯	⋯	⋯	⋯
	3	$35^m11^s.804440$	1	$21'49''.26656$	78	⋯	⋯	⋯	⋯
	4	$35^m11^s.804558$	1	$21'49''.26779$	48	⋯	⋯	⋯	⋯
70	3	$35^m11^s.955534$	7	$20'32''.36771$	280	⋯	⋯	⋯	⋯
72	3	$35^m12^s.049462$	8	$22'12''.07822$	315	⋯	⋯	⋯	⋯
75	4	$35^m12^s.141226$	1	$24'33''.46621$	106	⋯	⋯	⋯	⋯
86	$2+3$	$35^m12^s.600988$	7	$21'45''.50568$	265	⋯	⋯	⋯	⋯
93	1	$35^m12^s.847280$	7	$21'33''.97869$	244	⋯	⋯	⋯	⋯
98	1	$35^m12^s.964607$	6	$23'54''.70582$	204	⋯	⋯	⋯	⋯
122	3	$35^m13^s.428370$	14	$22'52''.27556$	228	⋯	⋯	⋯	⋯
127	3	$35^m13^s.506072$	12	$22'19''.94996$	360	⋯	⋯	⋯	⋯
129	3	$35^m13^s.529464$	5	$21'12''.75039$	231	⋯	⋯	⋯	⋯
130	1	$35^m13^s.586150$	13	$23'55''.26292$	456	⋯	⋯	⋯	⋯
	2	$35^m13^s.586319$	2	$23'55''.26712$	111	⋯	⋯	⋯	⋯
	3	$35^m13^s.586308$	1	$23'55''.26701$	60	⋯	⋯	⋯	⋯
	4	$35^m13^s.586438$	1	$23'55''.26861$	33	⋯	⋯	⋯	⋯
133	3	$35^m13^s.646517$	6	$24'09''.10777$	295	⋯	⋯	⋯	⋯
135	2	$35^m13^s.702626$	5	$21'49''.17879$	260	⋯	⋯	⋯	⋯
137	3	$35^m13^s.708093$	5	$25'08''.17479$	265	⋯	⋯	⋯	⋯
	4	$35^m13^s.708136$	5	$25'08''.21691$	314	⋯	⋯	⋯	⋯
148	2	$35^m13^s.957145$	11	$23'20''.47154$	501	⋯	⋯	⋯	⋯
149	$2+3$	$35^m13^s.903353$	5	$24'09''.28667$	278	⋯	⋯	⋯	⋯
154	1	$35^m13^s.972262$	4	$24'09''.84011$	149	⋯	⋯	⋯	⋯
	3	$35^m13^s.972311$	7	$24'09''.83995$	310	⋯	⋯	⋯	⋯
	4	$35^m13^s.972375$	1	$24'09''.83914$	40	⋯	⋯	⋯	⋯
158	2	$35^m14^s.054152$	11	$23'38''.45757$	428	3017363960251335424	10.7 ± 0.8	-7.1 ± 0.8	-7.9 ± 0.8
	4	$35^m14^s.054327$	4	$23'38''.45545$	320	⋯	⋯	⋯	⋯
161	1	$35^m14^s.058854$	33	$20'12''.573445$	518	⋯	⋯	⋯	⋯
167	4	$35^m14^s.196172$	3	$26'21''.14518$	241	⋯	⋯	⋯	⋯
170	4	$35^m14^s.262925$	4	$22'35''.45441$	196	⋯	⋯	⋯	⋯
176	4	$35^m14^s.339783$	3	$21'17''.44629$	219	⋯	⋯	⋯	⋯
177-1	1	$35^m14^s.335495$	9	$23'17''.42271$	373	⋯	⋯	⋯	⋯
	4	$35^m14^s.336155$	2	$23'17''.42214$	216	⋯	⋯	⋯	⋯
177-2	4	$35^m14^s.335835$	1	$23'17''.39939$	56	⋯	⋯	⋯	⋯
182	3	$35^m14^s.424573$	9	$21'26''.70387$	344	⋯	⋯	⋯	⋯
184	1	$35^m14^s.501740$	14	$22'38''.69711$	459	⋯	⋯	⋯	⋯
	2	$35^m14^s.501784$	4	$22'38''.70306$	212	⋯	⋯	⋯	⋯
	3	$35^m14^s.501787$	6	$22'38''.70296$	264	⋯	⋯	⋯	⋯
	4	$35^m14^s.501883$	1	$22'38''.70192$	52	⋯	⋯	⋯	⋯
188	2	$35^m14^s.505056$	11	$23'10''.34936$	403	⋯	⋯	⋯	⋯
189	1	$35^m14^s.545411$	9	$23'15''.99164$	267	⋯	⋯	⋯	⋯
196	1	$35^m14^s.655810$	4	$22'33''.74156$	152	3017364132048871168	17.9 ± 0.2	-16.7 ± 0.2	6.5 ± 0.2

Table 2
(Continued)

[FRM2016]	Epoch	α_{J2000} 5^h	σ_α μs	δ_{J2000} $-5°$	σ_δ μas	*Gaia* ID	$\Delta\theta$ (mas)	$\Delta\alpha$ (mas)	$\Delta\delta$ (mas)
197	2	$35^m14^s.646950$	5	20′42.″23801	260	3017365918756031744	173.8 ± 2.1	-165.6 ± 2.1	52.7 ± 1.8
198	3	$35^m14^s.665959$	10	22′11.″28275	348	⋯	⋯	⋯	⋯
	4	$35^m14^s.665154$	3	22′11.″28841	215	⋯	⋯	⋯	⋯
203	2 + 3	$35^m14^s.731189$	4	22′29.″82403	296	⋯	⋯	⋯	⋯
205	1	$35^m14^s.794851$	20	21′53.″89877	497	⋯	⋯	⋯	⋯
211	1	$35^m14^s.898525$	11	22′25.″40704	380	⋯	⋯	⋯	⋯
	2	$35^m14^s.898318$	3	22′25.″41142	153	⋯	⋯	⋯	⋯
	3	$35^m14^s.898317$	2	22′25.″41168	134	⋯	⋯	⋯	⋯
	4	$35^m14^s.898408$	3	22′25.″41948	280	⋯	⋯	⋯	⋯
212	1	$35^m14^s.916016$	2	22′39.″20577	82	3017364127743283584	25.6 ± 0.3	-25.3 ± 0.3	4.2 ± 0.2
222	3	$35^m15^s.234278$	12	22′56.″71107	356	⋯	⋯	⋯	⋯
227	3	$35^m15^s.340230$	8	22′18.″22981	361	⋯	⋯	⋯	⋯
230	4	$35^m15^s.393924$	6	22′33.″11715	149	⋯	⋯	⋯	⋯
232	4	$35^m15^s.391542$	4	22′29.″88937	214	⋯	⋯	⋯	⋯
240	1	$35^m15^s.521395$	5	23′37.″49236	271	⋯	⋯	⋯	⋯
241	1	$35^m15^s.555065$	4	25′14.″12514	144	3017360966647238272	1.3 ± 0.2	-0.2 ± 0.2	1.3 ± 0.2
	2	$35^m15^s.555280$	2	25′14.″12257	130	⋯	⋯	⋯	⋯
	3[b]	$35^m15^s.555262$	13	25′14.″12239	444	⋯	⋯	⋯	⋯
	4	$35^m15^s.555413$	1	25′14.″12075	47	⋯	⋯	⋯	⋯
242	2 + 3	$35^m15^s.588076$	12	21′26.″87028	382	⋯	⋯	⋯	⋯
249	4	$35^m15^s.749637$	6	23′38.″74543	302	⋯	⋯	⋯	⋯
250	1	$35^m15^s.773727$	2	23′09.″87026	81	3017364127743288704	1.0 ± 0.2	-0.3 ± 0.2	1.0 ± 0.2
	2	$35^m15^s.773899$	1	23′09.″86841	86	⋯	⋯	⋯	⋯
	3	$35^m15^s.773902$	1	23′09.″86840	65	⋯	⋯	⋯	⋯
	4	$35^m15^s.773989$	1	23′09.″86683	39	⋯	⋯	⋯	⋯
254	1	$35^m15^s.829235$	2	23′14.″15060	72	3017364132050194688	183.8 ± 0.2	33.8 ± 0.2	180.6 ± 0.2
	2	$35^m15^s.829898$	1	23′14.″15607	67	⋯	⋯	⋯	⋯
	3	$35^m15^s.829878$	1	23′14.″15598	72	⋯	⋯	⋯	⋯
	4	$35^m15^s.830213$	1	23′14.″15819	34	⋯	⋯	⋯	⋯
273	4	$35^m16^s.096551$	2	23′27.″94239	171	⋯	⋯	⋯	⋯
285	2 + 3	$35^m16^s.184889$	3	21′32.″84282	192	⋯	⋯	⋯	⋯
300	1	$35^m16^s.356075$	5	24′02.″82463	309	⋯	⋯	⋯	⋯
303	3	$35^m16^s.411129$	8	22′12.″37498	406	⋯	⋯	⋯	⋯
314	1	$35^m16^s.642910$	8	20′26.″63953	330	⋯	⋯	⋯	⋯
319	1	$35^m16^s.766695$	7	24′04.″25260	284	3017363955944478976	12.7 ± 0.4	-4.3 ± 0.4	-12.0 ± 0.4
	2	$35^m16^s.766633$	7	24′04.″24963	341	⋯	⋯	⋯	⋯
	3	$35^m16^s.766632$	10	24′04.″24969	389	⋯	⋯	⋯	⋯
	4	$35^m16^s.766638$	3	24′04.″24756	254	⋯	⋯	⋯	⋯
321	2	$35^m16^s.738295$	17	23′28.″30463	446	⋯	⋯	⋯	⋯
326	3	$35^m16^s.935631$	4	22′10.″22981	225	⋯	⋯	⋯	⋯
327	1	$35^m16^s.983560$	15	23′33.″02930	409	⋯	⋯	⋯	⋯
335	2	$35^m17^s.042397$	10	23′39.″63166	416	⋯	⋯	⋯	⋯
339	4	$35^m17^s.121826$	8	24′34.″50190	238	⋯	⋯	⋯	⋯
343	1	$35^m17^s.220600$	15	21′31.″70144	423	3017364368261463936	11.3 ± 0.4	3.3 ± 0.3	10.8 ± 0.4
347	4	$35^m17^s.334877$	1	22′36.″12379	154	⋯	⋯	⋯	⋯
350	1	$35^m17^s.392308$	11	22′03.″62402	414	⋯	⋯	⋯	⋯
	2[b]	$35^m17^s.392548$	9	22′03.″62441	410	⋯	⋯	⋯	⋯
	4	$35^m17^s.392764$	1	22′03.″62460	146	⋯	⋯	⋯	⋯
357	2 + 3	$35^m17^s.503387$	23	21′06.″03158	575	⋯	⋯	⋯	⋯
360	**3**	$35^m17^s.529123$	13	21′45.″79922	665	⋯	⋯	⋯	⋯
364	3	$35^m17^s.677673$	6	23′41.″15188	244	⋯	⋯	⋯	⋯
367	2	$35^m17^s.710690$	5	24′43.″20288	322	⋯	⋯	⋯	⋯
373	2 + 3	$35^m17^s.869362$	16	22′15.″27217	868	⋯	⋯	⋯	⋯
378	1	$35^m17^s.952561$	2	22′45.″43436	80	3017364127743299328	1.0 ± 0.2	-0.5 ± 0.2	0.8 ± 0.2
	2	$35^m17^s.953051$	1	22′45.″42909	64	⋯	⋯	⋯	⋯
	3	$35^m17^s.953037$	1	22′45.″42902	67	⋯	⋯	⋯	⋯
	4	$35^m17^s.953269$	1	22′45.″42740	33	⋯	⋯	⋯	⋯
382	1[b]	$35^m18^s.030668$	12	22′05.″39440	605	3017364166397351296[a]	1.6 ± 0.8	1.1 ± 1.0	1.1 ± 0.8
	4	$35^m18^s.031363$	1	22′05.″40002	140	⋯	⋯	⋯	⋯
389	1	$35^m18^s.216537$	7	23′36.″05593	304	3017364063330467072	194.0 ± 0.3	123.7 ± 0.2	-149.5 ± 0.3
398	4	$35^m18^s.305932$	1	25′05.″71411	109	⋯	⋯	⋯	⋯
400	1	$35^m18^s.372944$	2	22′37.″42754	74	3017364162103039104	1.1 ± 0.2	-0.4 ± 0.2	1.0 ± 0.2
	2	$35^m18^s.373244$	1	22′37.″42642	72	⋯	⋯	⋯	⋯

Table 2
(Continued)

[FRM2016]	Epoch	α_{J2000} 5^h	σ_α μs	δ_{J2000} $-5°$	σ_δ μas	*Gaia* ID	$\Delta\theta$ (mas)	$\Delta\alpha$ (mas)	$\Delta\delta$ (mas)
	3	$35^m18^s.373239$	1	22′37.″42623	63	⋯	⋯	⋯	⋯
	4	$35^m18^s.373427$	1	22′37.″42542	32	⋯	⋯	⋯	⋯
402	4	$35^m18^s.388443$	2	20′20.″34921	202	3017365948809434624	4.3 ± 2.0	3.1 ± 2.4	-0.6 ± 2.7
408	3	$35^m18^s.550783$	12	21′27.″88721	288	⋯	⋯	⋯	⋯
414-1	1	$35^m18^s.660441$	4	20′33.″83380	184	⋯	⋯	⋯	⋯
	2	$35^m18^s.660697$	14	20′33.″83502	862	⋯	⋯	⋯	⋯
	4	$35^m18^s.660855$	4	20′33.″83662	257	⋯	⋯	⋯	⋯
414-2	3	$35^m18^s.673470$	3	20′33.″71209	187	3017365880089958912	11.6 ± 1.1	8.6 ± 1.2	7.7 ± 1.1
	4	$35^m18^s.673562$	1	20′33.″71145	97	⋯	⋯	⋯	⋯
426	3	$35^m18^s.979086$	7	25′08.″14860	305	⋯	⋯	⋯	⋯
435	3	$35^m19^s.213224$	4	22′50.″68184	183	3017364097690179712	1.1 ± 0.4	0.5 ± 0.6	0.8 ± 0.4
440	4	$35^m19^s.493670$	3	22′58.″86720	204	⋯	⋯	⋯	⋯
456	3	$35^m19^s.855122$	8	23′57.″55121	385	⋯	⋯	⋯	⋯
457	2	$35^m20^s.067807$	16	21′06.″22523	485	⋯	⋯	⋯	⋯
459	1	$35^m20^s.135592$	3	21′33.″63052	114	3017365643877358464	1.5 ± 0.2	-0.3 ± 0.2	1.5 ± 0.2
462	4	$35^m20^s.168294$	1	26′39.″08568	94	3017360313812222720	1.0 ± 0.3	-0.3 ± 0.4	0.9 ± 0.3
466	2	$35^m20^s.226344$	3	20′56.″81211	204	3017365884396345600	165.2 ± 3.7	42.7 ± 4.0	159.5 ± 3.7
	3	$35^m20^s.226344$	1	20′56.″81220	68	⋯	⋯	⋯	⋯
467	3	$35^m20^s.296851$	5	25′04.″46652	195	⋯	⋯	⋯	⋯
468	4	$35^m20^s.400552$	2	22′13.″62575	160	3017364162103048704	4.6 ± 0.6	4.1 ± 0.6	1.9 ± 0.5
470	4	$35^m20^s.481920$	31	24′20.″28599	851	⋯	⋯	⋯	⋯
477	4	$35^m20^s.665562$	13	22′45.″41051	659	⋯	⋯	⋯	⋯
480	1	$35^m20^s.725215$	11	21′44.″33936	396	3017365643879095040	36.1 ± 0.3	21.3 ± 0.2	29.2 ± 0.4
	4	$35^m20^s.724666$	1	21′44.″33392	97	⋯	⋯	⋯	⋯
485	1	$35^m21^s.049414$	3	23′49.″00528	132	3017361108393637120	0.5 ± 0.2	-0.4 ± 0.2	0.3 ± 0.2
	2	$35^m21^s.049475$	5	23′49.″00468	259	⋯	⋯	⋯	⋯
	3	$35^m21^s.049468$	2	23′49.″00431	103	⋯	⋯	⋯	⋯
	4	$35^m21^s.049575$	1	23′49.″00162	88	⋯	⋯	⋯	⋯
501	2	$35^m22^s.116650$	8	24′32.″31589	311	⋯	⋯	⋯	⋯
508	4	$35^m22^s.299739$	2	24′14.″14305	171	⋯	⋯	⋯	⋯
509	4	$35^m22^s.364446$	3	25′01.″99665	330	⋯	⋯	⋯	⋯
512	3	$35^m22^s.676241$	6	23′06.″17739	227	⋯	⋯	⋯	⋯
514	3	$35^m22^s.824118$	4	25′47.″67696	200	3017360730428788608	199.8 ± 1.5	-194.3 ± 1.5	-46.6 ± 1.2
515	4	$35^m22^s.877839$	4	24′57.″59939	273	⋯	⋯	⋯	⋯
520	4	$35^m23^s.495180$	9	20′01.″67517	406	3017365983169196416[a]	8.9 ± 4.6	4.3 ± 6.3	1.6 ± 6.3
521	1	$35^m23^s.596407$	19	25′26.″71826	594	⋯	⋯	⋯	⋯
522	3	$35^m23^s.680511$	8	23′46.″19317	360	⋯	⋯	⋯	⋯
525	2	$35^m23^s.953379$	7	25′09.″49805	261	⋯	⋯	⋯	⋯
526	1	$35^m24^s.016722$	19	23′14.″09561	579	⋯	⋯	⋯	⋯
527	3	$35^m24^s.273278$	7	25′18.″86354	268	⋯	⋯	⋯	⋯
530	4	$35^m24^s.468753$	3	24′00.″91711	179	⋯	⋯	⋯	⋯
534	3	$35^m24^s.853747$	4	21′00.″81741	169	⋯	⋯	⋯	⋯
535	4	$35^m25^s.015058$	4	24′38.″53626	205	⋯	⋯	⋯	⋯
537	2	$35^m25^s.088440$	4	23′46.″79491	204	3017361074033139200	10.2 ± 0.3	8.9 ± 0.3	-5.0 ± 0.4
547	3	$35^m26^s.397825$	2	25′00.″72346	142	3017360833515044480	95.5 ± 0.4	-66.8 ± 0.4	68.3 ± 0.4
552	3	$35^m29^s.588773$	8	23′12.″23421	276	⋯	⋯	⋯	⋯
555	2	$35^m31^s.445661$	8	25′16.″43957	480	⋯	⋯	⋯	⋯
557	3	$35^m14^s.950741$	7	23′39.″24439	324	3017363960237919616	15.1 ± 0.8	9.1 ± 0.9	-12.0 ± 0.8
	4	$35^m14^s.950932$	5	23′39.″24586	424	⋯	⋯	⋯	⋯

Notes. Columns are (left to right): Source number [from Forbrich et al. (2016)], epoch, J2000 right ascension and declination, both with uncertainties, *Gaia* ID, the total separation between the Gaia and VLBA positions and the separation in both coordinate directions. The separations are defined as: $\Delta\alpha = (\alpha_{VLBA} - \alpha_{Gaia\ DR2}) \cdot \cos\delta$, $\Delta\delta = (\delta_{VLBA} - \delta_{GaiaDR2})$ and $\Delta\theta = \sqrt{\Delta\alpha^2 + \Delta\delta^2}$.
[a] Source in Gaia DR2 catalog, no proper motion and parallaxes are given. The angular separations from the radio source are estimated using the positions in epoch 2015.5 as given in the Gaia DR2 archive. A Gaia ID source number is also listed when there is coincidence.
[b] Source detected at a level between 6.0–6.5 times the image's noise.

It is interesting to note that the two instruments trace two different populations of stellar sources. Gaia measures stars that are bright at optical wavelengths, have low extinction, and are not superimposed on bright nebulosity, while the VLBA observes (mostly) magnetically active stars. Moreover, the VLBA targets are not limited by the heavy dust obscuration of the BN-KL region. Thus, the astrometry derived from VLBA and Gaia data is complementary when studying the kinematics of the ONC and the BN/KL region close to it.

Table 3
Sources with Determined Proper Motions from VLBA Observations

			VLBA			Gaia DR2		
[FRM2016] (1)	Other Name (2)	Spectral Type[a] (3)	μ_α^* (mas yr^{-1}) (4)	μ_δ (mas yr^{-1}) (5)	$\Delta\theta$ (mas) (6)	μ_α^* (mas yr^{-1}) (7)	μ_δ (mas yr^{-1}) (8)	$M_{\rm low}$ ($M_\odot$) (9)
18[b]	COUP 338	⋯	8.59 ± 0.11	−13.40 ± 0.28	⋯	⋯	⋯	⋯
66	GMR A	⋯	1.38 ± 0.10	−1.21 ± 0.07	⋯	⋯	⋯	⋯
130	COUP 554	⋯	1.43 ± 0.19	−1.76 ± 0.15	⋯	⋯	⋯	⋯
137	⋯	⋯	0.63 ± 0.19	−42.12 ± 0.44	⋯	⋯	⋯	⋯
154	COUP 594	⋯	0.54 ± 0.14	0.32 ± 0.13	⋯	⋯	⋯	⋯
158[b]	COUP 602	M3	2.62 ± 0.23	2.12 ± 0.55	10.7 ± 0.8	3.23 ± 0.32	1.25 ± 0.27	0.02
177-1[b]	COUP 625	⋯	3.28 ± 0.07	0.19 ± 0.15	⋯	⋯	⋯	⋯
184	GMR H	⋯	0.71 ± 0.28	−1.71 ± 0.91	⋯	⋯	⋯	⋯
198[b]	COUP 647	ORBS	−12.05 ± 0.21	−5.67 ± 0.43	⋯	⋯	⋯	⋯
211	GMR D	⋯	−0.76 ± 0.63	−3.76 ± 1.24	⋯	⋯	⋯	⋯
241	V1501 Ori	K4-M1	1.70 ± 0.12	1.46 ± 0.09	1.3 ± 0.2	1.22 ± 0.13	1.53 ± 0.11	⋯
250	θ^1 Ori E	B5-B8, G0-G5	1.31 ± 0.05	1.11 ± 0.14	1.0 ± 0.2	1.61 ± 0.12	1.23 ± 0.11	⋯
254	θ^1 Ori A_2	B1.5	4.87 ± 0.07	−2.56 ± 0.12	183.8 ± 0.2	1.54 ± 0.16	0.12 ± 0.14	5.6
319	V1279 Ori	K2-K6	−0.31 ± 0.12	1.66 ± 0.13	12.7 ± 0.4	1.92 ± 0.52	2.61 ± 0.43	0.12
350	COUP 874	⋯	2.23 ± 0.36	−0.20 ± 0.15	⋯	⋯	⋯	⋯
378	GMR G	G-K3	3.54 ± 0.08	2.38 ± 0.21	1.0 ± 0.2	3.77 ± 0.10	2.34 ± 0.08	⋯
382[b]	COUP 942	G-M2	3.46 ± 0.08	−1.88 ± 0.21	1.6 ± 0.8[c]	⋯	⋯	⋯
400	GMR F	G8-M2	2.38 ± 0.13	0.70 ± 0.08	1.1 ± 0.1	2.13 ± 0.10	0.78 ± 0.08	⋯
414-1	⋯	⋯	2.05 ± 0.08	−0.93 ± 0.11	⋯	⋯	⋯	⋯
414-2[b]	COUP 985	F8-K4	1.38 ± 0.15	0.64 ± 0.25	11.6 ± 1.2	−1.45 ± 0.52	−1.31 ± 0.43	⋯
480[b]	V1230 Ori	B1	−2.74 ± 0.07	1.81 ± 0.14	36.1 ± 0.4	2.60 ± 0.11	−1.72 ± 0.10	2.4
485	GMR V	G8-K5	0.74 ± 0.24	1.07 ± 0.52	0.4 ± 0.2	0.05 ± 0.12	−1.01 ± 0.11	⋯
557[b]	COUP 672	K5-M2	2.85 ± 0.20	−1.48 ± 0.55	15.1 ± 0.8	0.86 ± 0.37	0.55 ± 0.30	0.2

Notes. Columns are (left to right) source number from Forbrich et al. (2016), identification names from other surveys, spectral types from Hillenbrand et al. (2013), proper motions in R.A. and decl., both with uncertainties, total angular separation from Gaia DR2 sources, as given in Table 2, and their corresponding proper motions, and the mass lower limit estimated from the differences between VLBA and Gaia DR2 proper motions, as discussed in the text.

[a] Spectral types as reported by Hillenbrand et al. (2013), for multiple systems these do not necessarily represent the counterparts of the radio sources.

[b] Source detected only in two epochs. The errors may be underestimated.

[c] Source in Gaia DR2 catalog, no proper motion and parallaxes are given. The angular separations from the radio source are estimated using the positions in epoch 2015.5 as given in the Gaia DR2 archive.

4.1. Comparison with Gaia DR2 Results: Positions

We searched the Gaia DR2 catalog (Gaia Collaboration et al. 2018) for optical sources within 0.″2 of the position of radio sources and found 34 such cases. The search radius was chosen considering the possibility of tight multiple components, unidentified in previous observations with lower angular resolution. In order to determine the number of chance alignments between both catalogs within this separation, first we consider that the primary beam of the VLBA observations covers an area of $\sim 10^5$ arcsec^2, in which we have detected 126 radio sources. The total solid angle covered by our counterpart search is $126 \times (0.''2)^2 \times \pi \simeq 15.8$ arcsec^2. In the area covered by the VLBA primary beam there are 608 optical sources in the Gaia DR2 catalog. Thus, the number of Gaia DR2 sources projected onto our search area by chance is $608 \times (15.8/10^5) \simeq 0.1$.

The positions from Gaia DR2 catalog are determined for epoch 2015.50 (Gaia Collaboration et al. 2018). For a comparison with our VLBA data, the Gaia DR2 source positions and their errors have been extrapolated to the epoch of first detection of the corresponding radio source, including the effects of parallax. In the case of the VLBA detections related to source [FRM2016] 2, which are separated 20.6 mas, we do the extrapolation of the Gaia source to both detected epochs and compared the positions. The position difference with the source detected in epoch 4 is significantly smaller than for the source detected in epoch 3, indicating that the radio source detected in epoch 4 is related to the Gaia source. We will discuss source FRM2016] 2 in more detail in Section 4.5. The separations of the radio from the Gaia DR2 sources are listed in Table 2.

Since the position errors from both catalogs are below 1 mas, we expect the direct optical counterparts of radio sources to have radio versus optical separations of this magnitude. Only 11 of the 34 sources have separations less than 1.6 mas, while the remaining 23 sources have $\Delta\theta \geqslant 4.5$ mas. At the distance of the ONC, the radio emission from stellar coronae is expected to be unresolved by our VLBA observations. Even coronal flares and interactions between stellar coronae, which can reach distances of tens of stellar radii (e.g., Güdel 2002; Massi et al. 2008), would still be unresolved with our observations. Thus, separations $\Delta\theta \geqslant 4.5$ mas (or 1.8 au at the distance of the ONC) may be an indication that these 23 radio sources trace a stellar companion to the star seen at optical wavelengths. A clear example is θ^1 Ori A. Here the primary component, a B0.5-type star, dominates the optical emission and the strong radio source is a companion star, θ^1 Ori A_2 (Petr et al. 1998; Petr-Gotzens & Massi 2008; Gravity Collaboration et al. 2018). Gravity Collaboration et al. (2018) recently measured the separation between both components in three epochs spanning over 1.13 yr. A simple linear extrapolation of their measured relative positions to the epoch 2015.80 yields a total separation of 183.85 ± 0.12 mas, which is consistent with the estimated

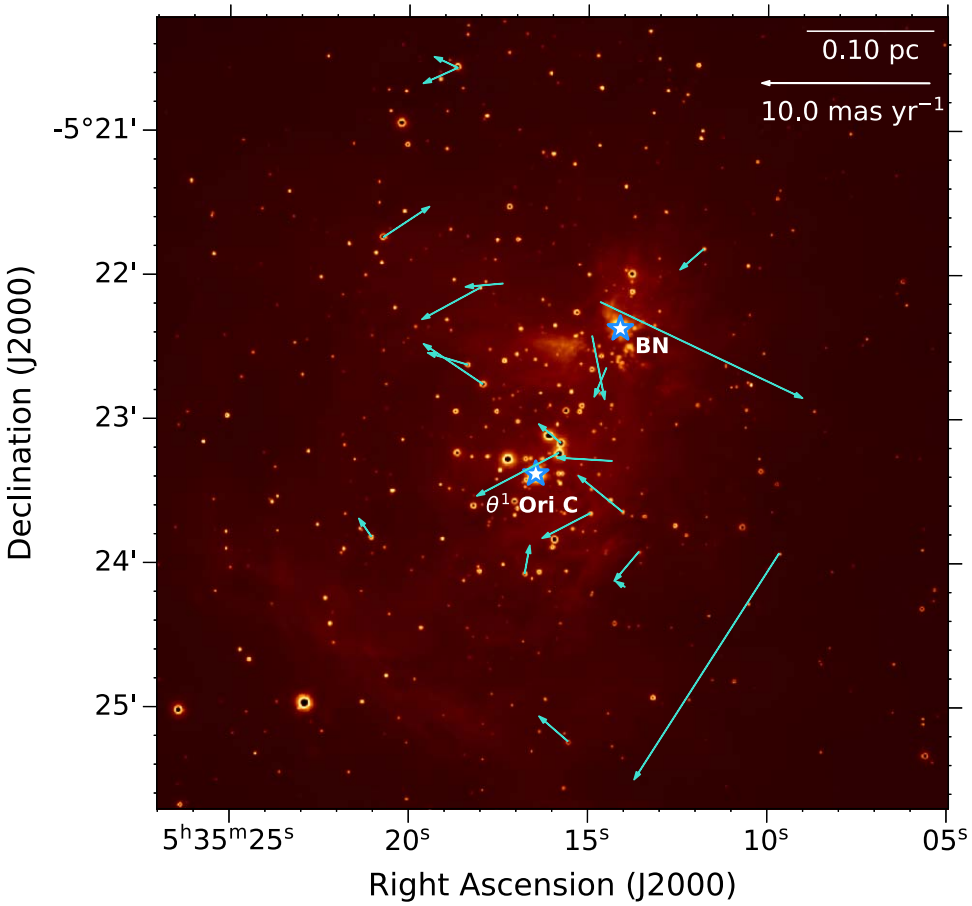

Figure 1. Background: VISION 2.1 μm image of the ONC (Meingast et al. 2016). Cyan arrows indicate the proper motion vectors of YSOs in the ONC-Trapezium region from Table 3, with the exception of source [FRM2016] 137 because of its very large nominal proper motion (see the text). The location of the two massive stars θ^1 Ori C and BN are indicated with blue stars.

separation between the radio and the Gaia DR2 source of $\Delta\theta = 183.8 \pm 0.2$ mas (see also Table 2 and Section 4.5 for a further discussion of this system).

The 11 radio sources with separations less than 1.6 mas could correspond to the true counterparts of the optical sources or to companions with separation $\leqslant$0.6 au (1 mas $\equiv$ 0.4 au). In Figure 2, we plot the distribution of the separations of radio and optical sources in both coordinates. We find that the weighted average of the separations in R.A. and decl. are $\overline{\Delta\alpha} = -0.32 \pm 0.15$(stat.) $\pm$ 0.16(sys.) mas and $\overline{\Delta\delta} = 0.99 \pm 0.10$(stat.) $\pm$ 0.16(sys.) mas, where the systematic uncertainty is associated with potential uncompensated ionospheric delays at the observing frequency of 7 GHz discussed in Section 2. The statistical errors were estimated using the formalism of the standard errors of mean. Thus, while the mean difference between the radio and optical positions in R.A. is consistent with no shift between the two catalogs, the decl. difference is statistically significant at the 5σ level.

In order to examine reference frame differences, we compile a list of quasars within a radius of 5° of the ONC that have accurate positions determined by Gaia DR2 and the VLBA (see Appendix A). We find that the mean position differences in R.A. and decl. are -0.6 ± 0.7 mas and 0.0 ± 0.6 mas, respectively. The observed systematic shift of 1.03 ± 0.16 mas for the ONC stars in decl. is larger than that seen for the quasars; however, the uncertainty in the quasar positions precludes a decisive test at this time. Similar studies, comparing VLBI and Gaia results, have been carried out for

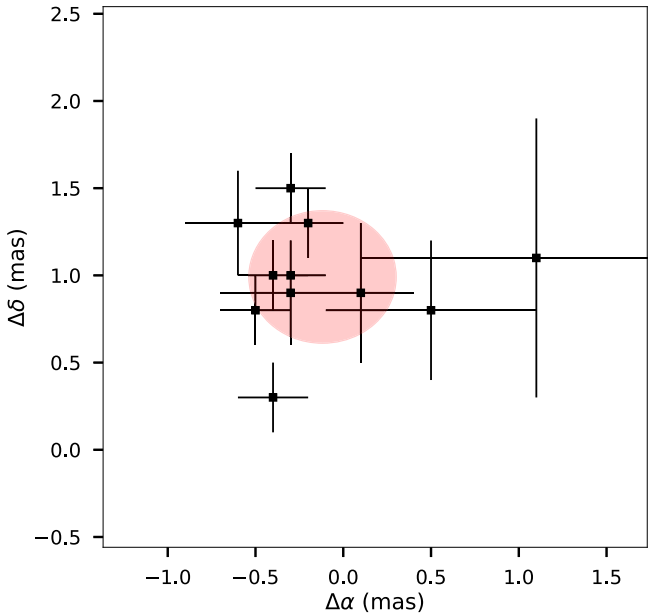

Figure 2. Comparison between VLBA and Gaia positions for the nine sources with total position separation <1.6 mas. The pink ellipse is centered in mean separations and its size correspond to two times the error values.

stellar parallaxes and proper motions (e.g., Xu et al. 2019), also finding differences between both catalogs. To our knowledge this has not yet been done for stellar positions. We conclude

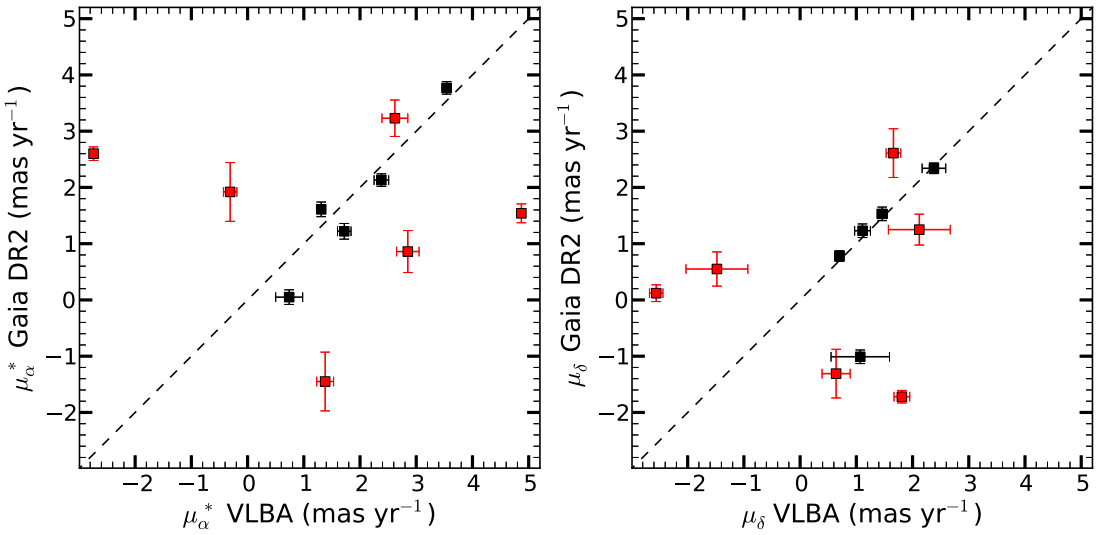

Figure 3. Comparison between VLBA and Gaia astrometry. Left: proper motion in R.A.. Right: proper motions in decl. Black symbols indicate sources where the difference in positions between VLBA and Gaia DR2 is less than 1.6 mas, otherwise the symbols are red.

that the origin of the stellar position difference in decl. between both catalogs remains uncertain.

4.2. Comparison with Gaia DR2 Results: Proper Motions

Of the 23 radio sources for which we have determined proper motions, 11 have a Gaia DR2 source within 0.″2, and with estimated proper motions. The Gaia DR2 proper motions and the separation between the radio source and the nearest optical counterpart are listed in Table 3 columns (6) to (8). In some cases, the radio sources and their nearest optical counterparts may not be directly associated as their separations are larger than 1.6 mas (see the previous section).

In Figure 3 we plot the Gaia DR2 proper motion of the nearest optical source against the VLBA proper motions. In this plot, black squares represent the sources for which $\Delta\theta \leqslant 1.6$ mas, and in red squares sources with $\Delta\theta > 1.6$ mas. There are six sources with radio minus optical position differences that are larger than 1.6 mas, and for these we find that the proper motions are also inconsistent in both coordinates (see Table 3 and Figure 3). In these cases, the radio source may trace a stellar companion to the star seen at optical wavelengths, rather than its direct counterpart.

Assuming that these seven pairs of radio-optical sources are binary systems and that relative motion between both components is dominated by the orbital motion, we may estimate a lower limit on the total mass of the system. Since the proper motions from Gaia DR2 and VLBA are not measured simultaneously, this analysis also implies that we are assuming that the orbital period of these candidate binaries is $\gg$3 yr, the time separation between the epoch of reported parameters for Gaia DR2 and our last radio observation. The total difference in proper motion, $\mu = \sqrt{(\mu^*_{\alpha,VLBA} - \mu^*_{\alpha,Gaia})^2 + (\mu_{\delta,\mathrm{VLBA}} - \mu_{\delta,Gaia})^2}$, in these plausible binaries, can be used to estimate a lower limit on the mass of the system. The orbital velocity, for a circular orbit, is given by $V = \sqrt{G \cdot M/a}$, where G is the gravitational constant, M is the total mass of the system, and a is the distance between binary components. The lower limit on mass is obtained assuming the orbit in the plane of the sky, then $M \geqslant a \cdot V^2/G$. Lower limits for V and a can be obtained from the proper motion and the angular separation. At the ONC distance, these parameters are V[km s^1] $= 1.9 \cdot \mu$[mas yr^{-1}], and a[km] $= 6 \times 10^7 \cdot \Delta\theta$[mas]. The lower limits in the system masses are listed in Table 3 column (9). Comparing these lower limits with the spectral type, we see that systems with early spectral types require larger lower limits, as would be expected for the binary system hypothesis.

From Figure 3 and Table 3, we find that for four of five stars with $\Delta\theta \leqslant 1.6$ mas, the differences of the radio and optical proper motions are smaller than three times the quadrature sum of their errors. The one outlier is source [FRM2016] 485 (also known as GMR V; Garay et al. 1987), whose VLBA and Gaia DR2 positions agree within 0.4 ± 0.2 mas, but the difference in proper motion in decl. is larger than five times the quadrature sum of errors. The weighted average differences for these four stars are -0.025 ± 0.080 mas yr^{-1} and -0.070 ± 0.090 mas yr^{-1}. Adopting three times the errors for limits, these results indicate upper limits of $\sim$0.3 mas yr^{-1} for the differences in proper motions measured with VLBA and Gaia DR2. These limits will improve when more proper motions of radio sources can be determined.

4.3. Comparison with Previous VLBA Results

Previous VLBA proper motion results for young stars in the ONC were obtained by Menten et al. (2007) and Kounkel et al. (2017). Menten et al. (2007) observed four young stars at four epochs spanning 1.5 yr, while Kounkel et al. (2017) obtained astrometric results for six young stars. These results are listed in Table 4. In order to compare the results of these studies with ours, we compute the weighted mean of absolute differences of proper motions ($\overline{|\Delta\mu^*_\alpha|}$, $\overline{|\Delta\mu_\delta|}$). The differences between the results of Menten et al. (2007) and ours are (0.3 ± 0.1, 0.7 ± 0.1) mas yr^{-1}, and a similar comparison for Kounkel et al. (2017) yields (0.2 ± 0.1, 0.2 ± 0.1) mas yr^{-1}. For the last value, we have omitted the proper motions derived for [FRM2016] 184, since the position changes are not consistent with a linear motion (see Section 4.5).

The results from the comparisons indicate that there are no significant differences with the measurements by Kounkel et al. (2017). On the other hand the differences with Menten et al. (2007), are significant at levels of 3.0 and 7.0 times the errors. [FRM2016] 254 and [FRM2016] 378 are known to be part of binary systems (Petr et al. 1998; Petr-Gotzens & Massi 2008;

Table 4
Previous Stellar Proper Motion (in mas yr^{-1}) Measurements in the ONC with VLBA

[FRM2016]	Other Name	This Work		Menten et al. (2007)		Kounkel et al. (2017)	
		μ_α^*	μ_δ	μ_α^*	μ_δ	μ_α^*	μ_δ
66	GMR A	1.38 ± 0.10	−1.21 ± 0.07	1.82 ± 0.09	−2.05 ± 0.18	1.81 ± 0.11	−1.60 ± 0.10
184	GMR H	0.71 ± 0.28	−1.71 ± 0.91	⋯	⋯	2.22 ± 0.18	−3.80 ± 0.55
250	θ^1 Ori E	1.31 ± 0.05	1.11 ± 0.14	⋯	⋯	1.45 ± 0.03	1.02 ± 0.08
254	θ^1 Ori A_2	4.87 ± 0.07	−2.56 ± 0.12	4.82 ± 0.09	−1.54 ± 0.18	4.81 ± 0.10	−2.53 ± 0.12
378	GMR G	3.54 ± 0.08	2.38 ± 0.21	4.29 ± 0.17	3.33 ± 0.37	3.82 ± 0.10	1.60 ± 0.17
400	GMR F	2.38 ± 0.13	0.70 ± 0.08	2.24 ± 0.09	0.66 ± 0.18	2.38 ± 0.08	0.55 ± 0.14

Note. Columns are (left to right) source number from Forbrich et al. (2016), identification names from other surveys, proper motions in R.A. and decl., both with uncertainties, from this work (see Table 3), Menten et al. (2007), and Kounkel et al. (2017).

Duchêne et al. 2018), and orbital motions will contribute to their final motions. The time separation between the observations reported by Menten et al. (2007) and ours is more than a decade, thus the difference between the proper motions of these sources, assumed lineal in both works, can be due to the effects of orbital motions. To our knowledge, neither [FRM2016] 400 or [FRM2016] 66 have been reported to be binary stars. However, the discrepancies of measured proper motions for [FRM2016] 66 may suggest that it could also be part of a binary or multiple system.

4.4. Trapezium Region Kinematics

Proper motions of radio emitting YSOs in the core of the ONC and the BN/KL region have been used to study the global motions and internal kinematics of these regions (Gómez et al. 2005; Dzib et al. 2017). These results used VLA observations spanning ∼30 yr and were mainly limited by the angular resolution of the VLA observations. With the higher angular resolution afforded by the VLBA, these results can be tested and significantly improved.

Using the VLBA proper motion values from Table 3, excluding sources [FRM2016] 18, 137, and 198 whose proper motions are significantly higher than the rest of the stars, we estimate the mean value of the proper motion ($\overline{\mu}$). In order to estimate the true proper motion dispersion (σ_μ), we correct the observed dispersion for measurement uncertainty as suggested by Jones & Walker (1988), i.e., $\sigma_\mu = \sigma_{\mu,Obs.} - \frac{1}{n}\sum_{i=1}^{n}\mu_{\rm err,i}^2$. For comparison, we have also estimated these parameters for stars in the Gaia DR2 catalog. Restricting our analysis to stars located in the coverage of our radio observations, with a parallax in the range from 2.4 to 2.6 mas (i.e., distances between 380 and 420 pc), and with Renormalized Unit Weight Error (RUWE[6]) values smaller than 1.4, we used 12 stars for the calculations (see Figure 4). Finally, as the astrometric precision from VLBA observations and the Gaia mission are comparable we estimated $\overline{\mu}$ and σ_μ combining these data sets. The results are shown in Table 5, together with those obtained by Dzib et al. (2017).

The averaged proper motions in the R.A. direction are consistent with a value of ∼1.0 mas yr^{-1} in the different data sets. For the decl. direction both the VLBA and Gaia DR2 data sets show motions near 0.0 mas yr^{-1}, contrary to the larger value of −0.8 mas yr^{-1} obtained with the VLA.

[6] The RUWE parameter is a quality indicator of Gaia DR2 fits. A RUWE value of 1.0 is expected for sources whose motion is consistent with the motion of a single star. Larger values may suggest that the source does not have good fit solutions, i.e., the star may not be single. More information is given on the Gaia webpage: https://gea.esac.esa.int/archive/documentation/GDR2/Gaia_archive/chap_datamodel/sec_dm_main_tables/ssec_dm_ruwe.html.

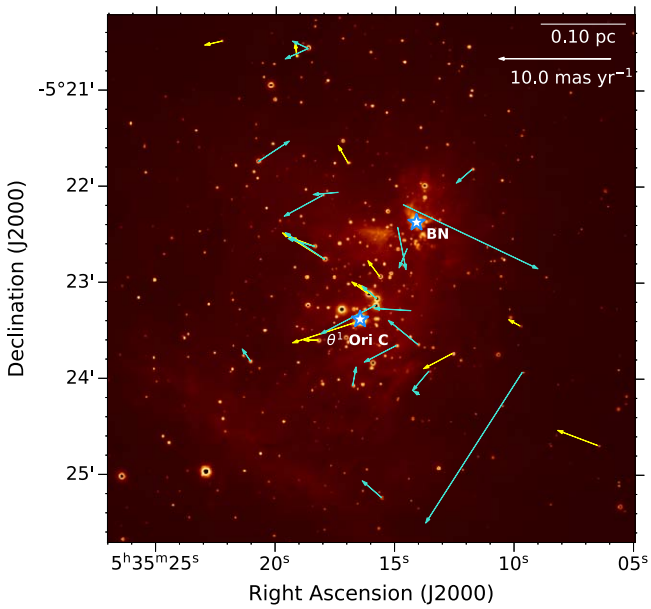

Figure 4. Same as Figure 1, but including in yellow arrows all the proper motions from Gaia DR2 catalog with RUWE ⩽ 1.4 in the same region of our study.

The proper motion dispersions for the VLA and Gaia data sets are close to a value of 1.0 mas yr^{-1} in both directions. Similar values were also found by Jones & Walker (1988) for optical stars covering a larger area of the ONC. Recent values of proper motion dispersions in the ONC have been estimated at optical and near-infrared, to be (σ_α, σ_δ) = (0.73 ± 0.05, 1.12 ± 0.10) mas yr^{-1} using Gaia DR2 data (Kuhn et al. 2019); (σ_α, σ_δ) = (0.83 ± 0.02, 1.12 ± 0.03) mas yr^{-1} using HST and Keck II NIRC2 data (Kim et al. 2019); (σ_α, σ_δ) = (0.89 ± 0.03, 1.21 ± 0.04) mas yr^{-1} using HST data (Platais et al. 2020). In the case of the VLBA data set the proper motion dispersion values are slightly larger. The large dispersions of VLBA proper motions could reflect the multiplicity of systems related to detected radio sources. Because of its high angular resolution imaging capability, the observations with the VLBA can trace individual motions in these systems, while the observations at optical, infrared, and the low-resolution observations at radio frequencies will trace some intensity-weighted motion of the system.

Finally, we have also searched for signatures of expansion and contraction in the cluster following the analysis techniques of Dzib et al. (2017; see also Rivera et al. 2015). These authors used the mean values of the dot and cross products of a unit

Table 5
Kinematics of the Trapezium

Data Set	$\overline{\mu_\alpha^*}$ (mas yr^{-1})	$\overline{\mu_\delta}$ (mas yr^{-1})	$\sigma_{\mu\alpha}$ (mas yr^{-1})	σ_{μ_δ} (mas yr^{-1})	σ_{v_α}[a] (km s^{-1})	σ_{v_δ}[a] (km s^{-1})	$\overline{\vec{v}\cdot\hat{r}}$ (km s^{-1})	$\overline{\vec{v}\times\hat{r}}$ (km s^{-1})
VLA[b]	1.0 ± 0.1	-0.8 ± 0.2	1.1 ± 0.1	1.3 ± 0.2	2.1 ± 0.2	2.5 ± 0.4	0.7 ± 0.3	-0.1 ± 0.3
VLBA	1.6 ± 0.2	0.1 ± 0.2	1.4 ± 0.2	1.7 ± 0.2	2.7 ± 0.4	3.2 ± 0.4	-0.8 ± 1.1	0.5 ± 1.1
Gaia	1.1 ± 0.1	0.2 ± 0.1	0.7 ± 0.1	1.2 ± 0.1	1.3 ± 0.2	2.2 ± 0.2	0.2 ± 2.3	0.8 ± 1.9
VLBA+Gaia[c]	1.20 ± 0.09	0.18 ± 0.09	0.84 ± 0.09	1.30 ± 0.09	1.60 ± 0.17	2.47 ± 0.17	-0.61 ± 1.00	0.57 ± 0.95

Notes. Columns are (left to right) proper motions data set, mean of proper motions, proper motion dispersions, velocity dispersions (all three parameters in R.A. and decl. and with their uncertainties), mean of dot and cross products of the unit vector and velocity vectors, both with their uncertainties.
[a] At a distance of 400 pc: 1.0 mas yr$^{-1} \equiv 1.9$ km s^{-1}.
[b] Values from Dzib et al. (2017).
[c] Values are the variance weighted average from the independent results of VLBA and Gaia data sets.

vector from the cluster center toward star positions ($\hat{r} = r/||r||$) and the velocity vector (v_*) of the individual stars. Large values in these products may indicate organized motion (see Rivera et al. 2015 for a discussion). For our analysis, the cluster center is defined as the average position of the stars with proper motion observed with the VLBA and the stars from Gaia with RUWE $\leqslant 1.4$; to be $(\alpha_0,\ \delta_0) = (5^{\rm h}35^{\rm m}16\overset{\rm s}{.}3,\ -5°22'58\overset{''}{.}6)$.[7] From Table 5 we noticed that in all the cases $\vec{v}\cdot\hat{r}$ and $\vec{v}\times\hat{r}$ are consistent with 0.0 km s^{-1} within two times their uncertainties. Even with our higher-resolution astrometry data, we find no strong evidence of rotation, contraction, or expansion of the cluster, in line with previous results.

4.5. Individual Sources

While most of the stars show proper motions within 2σ of the mean motion components, four sources have motions well outside this range: [FRM2016] 18, 137, 198, and 211.

Formally sources [FRM2016] 18, 137, and 198 exhibit the largest proper motions in our sample. Their proper motions are equivalent to velocities of 30, 80, and 25 km s^{-1}). Previous radio proper motions of source [FRM2016] 198 were estimated by Dzib et al. (2017),[8] to be $(-2.1 \pm 3.0,\ -0.9 \pm 1.4)$ mas yr^{-1}, which are considerably lower than our values. Even with the lower resolution of the VLA Dzib et al. (2017) would have detected such large proper motions. Since the VLBA proper motions are based on detections in only two epochs, and allowing for the highly variable nature of the emission, it is likely that [FRM2016] 198 is a binary system with a separation of $\sim$10 mas, and the detections in the two epochs correspond to different stars. The large proper motion measured for sources [FRM2016] 18 and 137 are intriguing, since they are well above the proper motions exhibited for most of the stars in the ONC. However, with only two detections there is still the open possibility that they correspond to different stellar components in multiple systems. Future multiepoch and deep VLBA observations, as those presented in this work, will help to clarify the nature of the measured motions from the present observations.

[FRM2016] 211 was detected as a single source in the four observations. In order to obtain a reduced $\chi^2 = 1.0$ in the proper motion fitting, we needed to add in quadrature values 1.2 and 2.4 mas to the R.A. and decl. position errors. These values are much larger than the expected systematic errors for VLBA observations, and, indeed, no other ONC star shows such large uncertainties. We suggest two explanations: (1) the motion of [FRM2016] 211 is nonlinear, or (2) we are detecting different stars among the observations. Both explanations point to a binary nature of this system.

In our images we identify two compact radio sources in the direction of sources [FRM2016] 414 and [FRM2016] 177, which have not been reported as binaries before. Both sources show X-ray emission (see Paper I), and the spectral type of [FRM2016] 414 is F8–K4 (Hillenbrand et al. 2013). The separation between the radio emission from stars in these system are $0\overset{''}{.}22$ and $0\overset{''}{.}023$ for [FRM2016] 414 and [FRM2016] 177, respectively. With the current data it is not possible to constrain if they form gravitationally bound binaries, but further astrometric studies of these objects can determine this. At high resolution, such a study will only be possible with VLBI techniques, as they are not detected at optical or NIR wavelengths.

In the direction of the VLA source [FRM2016] 2, we have single detections in epochs 3 and 4; i.e., with a time baseline of 1 yr. The separation between the radio sources is 20.6 mas. Assuming that both radio sources are the same star would imply a large proper motion of 20.6 mas yr^{-1} ($\simeq$39 km s^{-1}). However, the Gaia source associated with this source has a proper motion of $(\mu_\alpha*,\ \mu_\delta) = (1.64 \pm 0.08,\ 0.07 \pm 0.07)$ mas yr^{-1}, inconsistent with a source with fast motion. Furthermore, extrapolating the 2015.5 position of the Gaia source to epochs 3 (2017.8) and 4 (2018.8), find it to be separated 22.6 ± 0.3 mas and 1.6 ± 0.3 mas from the radio sources detected in epochs 3 and 4, respectively, suggesting that only the source detected in epoch 4 is probably directly related to the optical source. Our conclusion for [FRM2016] 2 is that the two radio sources detected in the two different epochs are not the same.

Toward the VLA source [FRM2016] 184, we detected single sources in all four epochs. The proper motion using the four epochs is $(\mu_\alpha*,\ \mu_\delta) = (0.71 \pm 0.28,\ -1.71 \pm 0.91)$ mas yr^{-1}, where we have added in quadrature additional values of 0.33 and 1.66 mas in R.A. and decl., respectively, to the position errors to obtain a $\chi^2 = 1$ in our fit. The detections in epochs 2 and 3 are consistent within errors as expected since the separation between the epochs is only one day, suggesting that the source in these epochs is the same. The measured proper motion between epochs 1 and 2 + 3 is $(\mu_\alpha*,\ \mu_\delta) = (0.34 \pm 0.19,\ -2.95 \pm 0.26)$ mas yr^{-1}, while the proper motion from epochs 2 + 3 and 4 is $(\mu_\alpha*,\ \mu_\delta) = (1.46 \pm 0.20,\ 1.11 \pm 0.18)$ mas yr^{-1}. Furthermore, these motions are

[7] The independent cluster center values for the used stars from the Gaia and VLBA catalog are 9″ away from this position.
[8] Source named as VLA J053514.66−052211.2 by these authors.

different from the proper motions reported by Kounkel et al. (2017), who also used VLBA observations. The motion related to [FRM2016] 184 deserves further investigation to clarify its unusual motion.

θ^1 Ori A is a hierarchical triple system known to have a total mass of $\sim$20 $M_\odot$. At optical wavelengths, the brightest component is θ^1 Ori A_1, which is a tight binary itself ($P = 65.433$ days, Lloyd & Stickland 1999; Bondar' et al. 2000), composed of a $\approx$15 $M_\odot$, massive star (Weigelt et al. 1999; Schertl et al. 2003; Simón-Díaz et al. 2006; Nieva & Przybilla 2014) and a T-Tauri star of $\approx$2.5 $M_\odot$ (Bossi et al. 1989). At an angular distance of 0.″18 from the tight binary, there is the 4 $M_\odot$ star θ^1 Ori A_2 (Petr et al. 1998). NIR interferometry data taken from 1994 to 2010 and analyzed by Grellmann et al. (2013) indicated linear movement of A_2 relative to A_1 suggesting unbound motion. However, adding new NIR interferometry data taken between 2016 and 2018, the relative motions determined by Gravity Collaboration et al. (2018) strongly suggest that θ^1 Ori A_2 is gravitationally bound to the tight binary θ^1 Ori A_1. As discussed before, the optical source seen by Gaia DR2 is related to component A_1, and the radio source is related to component A_2. The total differences between the VLBA and Gaia DR2 proper motions is 4.3 ± 0.2 mas yr^{-1}, which at the distance of the ONC is equivalent to a velocity of 8.2 ± 0.4 km s^{-1}. Assuming, in a simplifying estimate, a circular orbit for the system, the escape velocity of A_2 from A_1, with a total mass of 18 $M_\odot$, is 21 km s^{-1}. This would indicate indeed that the system is bound, as the relative velocity between the components would be significantly smaller than the escape velocity.

5. Conclusions

We have imaged 126 compact nonthermal radio sources near the Trapezium in the ONC using data acquired with VLBA observations over a 3 yr period. The positions of 34 radio detected sources were found within 0.″2 of a Gaia DR2 star. Most of the Gaia DR2 sources (23) are well separated (>4 mas) from the associated radio source, indicating that the optical and the radio source are not the same star. We argue that the radio sources could be lower-mass companions of the stars seen by Gaia. For the remaining 11 cases, the separation is <1.6 mas and could indicate that both telescopes observe the same stellar sources. We find mean separations of $-0.32 \pm 0.15 \pm 0.16$ mas and $0.99 \pm 0.10 \pm 0.16$ mas in R.A. and decl., respectively. The stellar position difference in decl. between both catalogs is significant at a level of 5σ. Its origin is still uncertain, but it could conceivably be due to unidentified binaries in the sample. For three targets, two separate components were identified in the images, further expanding the discovery space for previously unknown multiple systems in the ONC.

Radio proper motions were estimated for 23 YSOs with accuracies of $\approx$0.1 mas yr^{-1}, similar to Gaia accuracy. Within 1.6 mas, five of them have a counterpart in the Gaia DR2 catalog, and by comparing their proper motions from both catalogs, we found differences of -0.025 ± 0.080 and -0.070 ± 0.090 mas yr^{-1} in R.A. and decl., respectively.

By combining proper motions from Gaia DR2 and VLBA we have improved the values of the global motions and the kinematic of the ONC core. The global proper motion and velocity dispersion are $(\mu_\alpha^*, \mu_\delta) = (1.20 \pm 0.09,\ 0.18 \pm 0.09)$ mas yr^{-1} and $(\sigma_{\mu_\alpha^*}, \sigma_{\mu_\delta}) = (0.84 \pm 0.09,\ 1.30 \pm 0.09)$ mas yr^{-1}, respectively. The search of ordered motion through vector products $\overline{\boldsymbol{v} \cdot \hat{\boldsymbol{r}}}$ and $\overline{\boldsymbol{v} \times \hat{\boldsymbol{r}}}$ show that the obtained values are consistent with a value of 0.0 km s^{-1} within two times the errors. These results do not show indications of expansion/contraction or rotation of the young stellar cluster.

The National Radio Astronomy Observatory is a facility of the National Science Foundation operated under cooperative agreement by Associated Universities, Inc.

This work has made use of data from the European Space Agency (ESA) mission Gaia (https://www.cosmos.esa.int/gaia), processed by the Gaia Data Processing and Analysis Consortium (DPAC, https://www.cosmos.esa.int/web/gaia/dpac/consortium). Funding for the DPAC has been provided by national institutions, in particular the institutions participating in the Gaia Multilateral Agreement.

Facility: VLBA.

Appendix A
VLBA and Gaia DR2 Position Differences of Extragalactic Sources around the ONC

We searched for extragalactic sources in a radius of 5° around the ONC that have compact radio emission and that are also in the Gaia DR2 catalog. We found eight sources meeting these requirements and list them in Table 6. Their most recently determined radio positions and their uncertainties were taken from the AstroGeo catalog ***rfc_2020c***[9] and are shown in Table 6. The difference between the position of each radio source and that of its Gaia DR2 counterpart is also shown in Table 6.

Previous comparisons of the positions of compact extragalactic objects based on data from Very Long Baseline Interferometry and the Gaia satellite have found that around 10% of them have significant offsets between them (Petrov & Kovalev 2017; Petrov et al. 2019). These differences have a physical origin and are mainly due the spatially different appearance of optical and radio jets, which both evolve with time (see the discussion by Petrov et al. 2019). Statistically, we expect that 0.8 sources from our sample are part of this group. In our sample, source J0552−0727 has a significant separation of 28.4 mas, and was thus omitted from our analysis.

The statistical analysis of the separation of the remaining sources yield mean separations of $(\Delta\alpha, \Delta\delta) = (-0.6 \pm 0.7,\ 0.0 \pm 0.6)$ mas that have standard deviations of $(\sigma_{\Delta\alpha}, \sigma_{\Delta\delta}) = (1.8,\ 1.4)$ mas. The mean separation of our sample is smaller than the median separation found by Petrov & Kovalev (2017) for VLBI and Gaia DR1 positions. However, the large dispersion in the values may suggest differences between the radio and Gaia DR2 reference frames.

[9] http://astrogeo.org/rfc/

Table 6
Positions at Radio Frequencies of Extragalactic Sources around the ONC and Their Separations from Gaia DR2

Name	α_{J2000}	σ_α μs	δ_{J2000}	σ_δ μas	Gaia ID (DR2)	$\Delta\alpha$ (mas)	$\Delta\delta$ (mas)
J0539−0514	$05^h39^m59\overset{s}{.}937139$	10	−05°14′41.″30061	280	3023327569572290688	−0.4 ± 0.2	−0.2 ± 0.3
J0529−0519	$05^h29^m53\overset{s}{.}533500$	7	−05°19′41.″61733	160	3209472860931863424	−2.0 ± 1.3	−0.9 ± 1.5
J0541−0541	$05^h41^m38\overset{s}{.}083368$	7	−05°41′49.″42846	110	3017106773301050240	+0.8 ± 1.5	+0.9 ± 1.4
J0532−0307	$05^h32^m07\overset{s}{.}519331$	8	−03°07′07.″03649	190	3216726171637867136	+0.7 ± 1.0	+2.9 ± 1.0
J0545−0539	$05^h45^m23\overset{s}{.}358039$	17	−05°39′37.″83964	350	3022323749816621568	−4.2 ± 0.5	−0.7 ± 0.8
J0522−0725	$05^h22^m23\overset{s}{.}196758$	52	−07°25′13.″48025	1180	3207290781323060096	+1.0 ± 0.8	−1.5 ± 1.2
J0517−0520	$05^h17^m28\overset{s}{.}110159$	8	−05°20′40.″84120	190	3208721928848872576	−0.1 ± 0.3	+0.2 ± 0.3
J0552−0727	$05^h52^m11\overset{s}{.}376231$	9	−07°27′22.″51824	250	3018834797558565376	+2.4 ± 1.0	−28.3 ± 1.1

Note. Columns are (left to right) source name, J2000 positions in R.A. and decl., both with uncertainties, Gaia ID, and separations between the Gaia and VLBA positions in both coordinate directions. The separations are defined as $\Delta\alpha = (\alpha_{\rm VLBA} - \alpha_{\rm Gaia\ DR2}) \cdot \cos\delta$ and $\Delta\delta = (\delta_{\rm VLBA} - \delta_{\rm Gaia\ DR2})$.

Table 7
Stars in the Gaia DR2 Catalog Used for the Estimation of Values in Table 5

Name	Sp. Type	Gaia ID (DR2)	RUWE	$\alpha_{J2015.5}$	σ_α μs	$\delta_{J2015.5}$	σ_δ μas	μ_α* (mas yr^{-1})	μ_δ (mas yr^{-1})
θ^1 Ori F	B8	3017364063331140224	1.0	$5^h35^m16\overset{s}{.}732576$	4	−5°23′25.″22448	60	5.45 ± 0.11	−1.77 ± 0.10
θ^1 Ori B	B1V	3017364132049943680	1.0	$5^h35^m16\overset{s}{.}135316$	3	−5°23′06.″76466	49	1.46 ± 0.11	1.03 ± 0.10
V2325 Ori	M0	3017364063330467072	1.4	$5^h35^m18\overset{s}{.}208086$	4	−5°23′35.″90580	52	1.32 ± 0.13	−0.00 ± 0.10
θ^1 Ori E	G2IV	3017364127743288704	1.2	$5^h35^m15\overset{s}{.}773584$	4	−5°23′09.″87097	72	1.61 ± 0.12	1.23 ± 0.11
V348 Ori	G8-K1	3017364127743288320	1.2	$5^h35^m15\overset{s}{.}636427$	3	−5°22′56.″43502	43	1.08 ± 0.12	1.45 ± 0.10
Brun 633	A4-A7	3017365880089961728	1.0	$5^h35^m19\overset{s}{.}139597$	2	−5°20′38.″72779	35	0.14 ± 0.08	1.20 ± 0.07
GMR G	K2	3017364127743299328	1.2	$5^h35^m17\overset{s}{.}952386$	3	−5°22′45.″4353	38	3.77 ± 0.10	2.34 ± 0.08
GMR F	K0	3017364162103039104	1.2	$5^h35^m18\overset{s}{.}372793$	3	−5°22′37.″42811	38	2.13 ± 0.10	0.78 ± 0.08
Brun 676	K3	3017365880089976064	1.0	$5^h35^m22\overset{s}{.}265125$	2	−5°20′29.″26229	34	1.56 ± 0.07	−0.36 ± 0.07
MR Ori	A2:Vv	3017364372568073472	0.9	$5^h35^m16\overset{s}{.}979192$	2	−5°21′45.″31264	33	0.90 ± 0.07	1.56 ± 0.06
LV Ori	K1V	3017364028971010432	1.2	$5^h35^m12\overset{s}{.}601447$	2	−5°23′44.″13115	38	2.57 ± 0.08	−1.36 ± 0.08
V1326 Ori	K8	3017363994611276032	1.1	$5^h35^m09\overset{s}{.}769407$	3	−5°23′26.″89052	37	1.02 ± 0.12	0.56 ± 0.09

Note. Columns are (left to right) source name, spectral type, Gaia ID in the DR2 catalog, Gaia DR2 positions in R.A. and decl. given in the epoch J2015.5, both with uncertainties, and proper motions in both coordinate directions.

Appendix B
Stars with Good Astrometry in Gaia DR2 and inside the Area of Our Radio Study

In this appendix we give a list of the stars in the Gaia DR2 catalog used for the estimation of values in Table 5. The criteria used to compile this list were as follows: to be in the same area as the primary beam of the VLBA observations, to have a measured parallax suggesting a distance between 380 and 420 pc, and to have a RUWE parameter $\leqslant$1.4. These stars are listed in Table 7 with their positions and proper motions.

ORCID iDs

Sergio A. Dzib https://orcid.org/0000-0001-6010-6200
Jan Forbrich https://orcid.org/0000-0001-8694-4966
Mark J. Reid https://orcid.org/0000-0001-7223-754X
Karl M. Menten https://orcid.org/0000-0001-6459-0669

References

Bondar', N. I., Vitrichenko, É. A., & Zakirov, M. M. 2000, AstL, 26, 452
Bossi, M., Gaspani, A., Scardia, M., & Tadini, M. 1989, A&A, 222, 117
Churchwell, E., Felli, M., Wood, D. O. S., & Massi, M. 1987, ApJ, 321, 516
Da Rio, N., Robberto, M., Hillenbrand, L. A., Henning, T., & Stassun, K. G. 2012, ApJ, 748, 14
Deller, A. T., Brisken, W. F., Phillips, C. J., et al. 2011, PASP, 123, 275
Duchêne, G., Lacour, S., Moraux, E., Goodwin, S., & Bouvier, J. 2018, MNRAS, 478, 1825
Dzib, S. A., Rodríguez, L. F., Loinard, L., et al. 2017, ApJ, 834, 139
Feigelson, E. D., & Montmerle, T. 1999, ARA&A, 37, 363
Forbrich, J., Dzib, S. A., Reid, M. J., & Menten, K. M. 2021, ApJ, 906, 23, (Paper I)
Forbrich, J., Menten, K. M., & Reid, M. J. 2008, A&A, 477, 267
Forbrich, J., Rivilla, V. M., Menten, K. M., et al. 2016, ApJ, 822, 93
Gaia Collaboration, Brown, A. G. A., Vallenari, A., et al. 2018, A&A, 616, A1
Garay, G., Moran, J. M., & Reid, M. J. 1987, ApJ, 314, 535
Genzel, R., & Stutzki, J. 1989, ARA&A, 27, 41
Getman, K. V., Feigelson, E. D., Grosso, N., et al. 2005, ApJS, 160, 353
Gómez, L., RodrÍguez, L. F., Loinard, L., et al. 2005, ApJ, 635, 1166
Gómez, L., Rodríguez, L. F., Loinard, L., et al. 2008, ApJ, 685, 333
Gravity Collaboration, Karl, M., Pfuhl, O., et al. 2018, A&A, 620, A116
Greisen, E. W. 2003, in Information Handling in Astronomy—Historical Vistas, Astrophysics and Space Science Library, Vol. 285, ed. A. Heck (Dordrecht: Kluwer Academic), 109
Grellmann, R., Preibisch, T., Ratzka, T., et al. 2013, A&A, 550, A82
Güdel, M. 2002, ARA&A, 40, 217
Hillenbrand, L. A. 1997, AJ, 113, 1733
Hillenbrand, L. A., Hoffer, A. S., & Herczeg, G. J. 2013, AJ, 146, 85
Hirota, T., Bushimata, T., Choi, Y. K., et al. 2007, PASJ, 59, 897
Jones, B. F., & Walker, M. F. 1988, AJ, 95, 1755
Kim, D., Lu, J. R., Konopacky, Q., et al. 2019, AJ, 157, 109
Kim, M. K., Hirota, T., Honma, M., et al. 2008, PASJ, 60, 991
Kounkel, M., Hartmann, L., Loinard, L., et al. 2014, ApJ, 790, 49
Kounkel, M., Hartmann, L., Loinard, L., et al. 2017, ApJ, 834, 142
Kuhn, M. A., Hillenbrand, L. A., Sills, A., Feigelson, E. D., & Getman, K. V. 2019, ApJ, 870, 32
Lloyd, C., & Stickland, D. J. 1999, IBVS, 4809, 1

Massi, M., Ros, E., Menten, K. M., et al. 2008, A&A, 480, 489
Meingast, S., Alves, J., Mardones, D., et al. 2016, A&A, 587, A153
Menten, K. M., & Reid, M. J. 1995, ApJL, 445, L157
Menten, K. M., Reid, M. J., Forbrich, J., & Brunthaler, A. 2007, A&A, 474, 515
Muench, A., Getman, K., Hillenbrand, L., & Preibisch, T. 2008, in Handbook of Star Forming Regions, Volume I: The Northern Sky, Vol. 4, ed. B. Reipurth (San Francisco, CA: ASP), 483
Nieva, M.-F., & Przybilla, N. 2014, A&A, 566, A7
Petr, M. G., Coudé du Foresto, V., Beckwith, S. V. W., Richichi, A., & McCaughrean, M. J. 1998, ApJ, 500, 825
Petr-Gotzens, M. G., & Massi, M. 2008, in Multiple Stars Across the H-R Diagram, ed. S. Hubrig, M. Petr-Gotzens, & A. Tokovinin (Berlin: Springer), 281
Petrov, L., & Kovalev, Y. Y. 2017, MNRAS, 467, L71
Petrov, L., Kovalev, Y. Y., & Plavin, A. V. 2019, MNRAS, 482, 3023
Platais, I., Robberto, M., Bellini, A., et al. 2020, AJ, 159, 272
Reid, M. J., Brunthaler, A., Menten, K. M., et al. 2017, AJ, 154, 63
Reid, M. J., & Honma, M. 2014, ARA&A, 52, 339
Rivera, J. L., Loinard, L., Dzib, S. A., et al. 2015, ApJ, 807, 119
Rodríguez, L. F., Dzib, S. A., Loinard, L., et al. 2017, ApJ, 834, 140
Rodríguez, L. F., Dzib, S. A., Zapata, L., et al. 2020, ApJ, 892, 82
Sandstrom, K. M., Peek, J. E. G., Bower, G. C., Bolatto, A. D., & Plambeck, R. L. 2007, ApJ, 667, 1161
Schertl, D., Balega, Y. Y., Preibisch, T., & Weigelt, G. 2003, A&A, 402, 267
Simón-Díaz, S., Herrero, A., Esteban, C., & Najarro, F. 2006, A&A, 448, 351
Weigelt, G., Balega, Y., Preibisch, T., et al. 1999, A&A, 347, L15
Xu, S., Zhang, B., Reid, M. J., Zheng, X., & Wang, G. 2019, ApJ, 875, 114
Zapata, L. A., Rodríguez, L. F., Kurtz, S. E., & O'Dell, C. R. 2004, AJ, 127, 2252
Zuckerman, B. 1973, ApJ, 183, 863